Article

Synthesis, Structure, and Dynamic Behavior of Cyclopentadienyl-Lithium, -Sodium, and -Potassium Annelated with Bicyclo[2.2.2]octene Units: A Systematic Study on Site Exchange of Alkali Metals on a Cyclopentadienyl Ring in Tetrahydrofuran

Tohru Nishinaga, Daisuke Yamazaki, Helmut Stahr, Atsushi Wakamiya, and Koichi Komatsu

J. Am. Chem. Soc., **2003**, 125 (24), 7324-7335• DOI: 10.1021/ja0346431 • Publication Date (Web): 22 May 2003

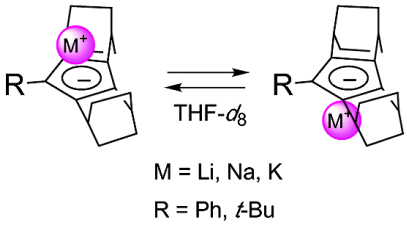

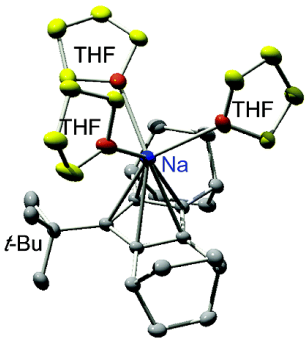

More About This Article

Additional resources and features associated with this article are available within the HTML version:

- Supporting Information
- Links to the 5 articles that cite this article, as of the time of this article download
- Access to high resolution figures
- Links to articles and content related to this article
- Copyright permission to reproduce figures and/or text from this article

View the Full Text HTML

J|A|C|S
ARTICLES
Published on Web 05/22/2003

Synthesis, Structure, and Dynamic Behavior of Cyclopentadienyl-Lithium, -Sodium, and -Potassium Annelated with Bicyclo[2.2.2]octene Units: A Systematic Study on Site Exchange of Alkali Metals on a Cyclopentadienyl Ring in Tetrahydrofuran

Tohru Nishinaga, Daisuke Yamazaki, Helmut Stahr, Atsushi Wakamiya, and Koichi Komatsu*

Contribution from Institute for Chemical Research, Kyoto University, Uji, Kyoto 611-0011, Japan

Received February 13, 2003; E-mail: komatsu@scl.kyoto-u.ac.jp

Abstract: Novel cyclopentadienyl (Cp)−alkali metal complexes **1**−M and **2**−M (M = Li, Na, K), in which the Cp ring is annelated with two bicyclo[2.2.2]octene units and substituted with a phenyl group for **1** and a *tert*-butyl group for **2**, were synthesized, and their structures and dynamic behaviors were investigated by means of X-ray crystallography, dynamic ^{13}C NMR, and DFT calculations. The X-ray crystallography results indicated that **1**−Li, **1**−Na, and **2**−Na form monomeric contact ion pairs (CIP) with three THF molecules coordinated to the metal atom. Also, in THF-d_8, all of the **1**−M and **2**−M form monomeric CIP in the ground state. However, variable-temperature ^{13}C NMR measurements of **1**−M and **2**−M in THF-d_8 demonstrated dynamic behavior in which the metal ion exchanges positions between the upper and lower faces of the Cp ring. From a study of the concentration dependence of the dynamic behavior, the exchange was found to proceed principally as an intramolecular process at concentration ranges lower than 0.2 M. The experimentally observed $\Delta G^{\ddagger}$ values for the intramolecular exchange process for all the **1**−M and **2**−M (except for **2**−Li, whose intramolecular process was too slow to observe) were found to be quite similar in THF-d_8 solution and to fall within the range of 12−14 kcal mol^{-1}. Within this range, a tendency was observed for the $\Delta G^{\ddagger}$ values to increase as the size of the metal decreased. Theoretical calculations (B3LYP/6-31G(d)) afforded considerably large values as the gas-phase dissociation energy for **1**−M (162.7 kcal mol^{-1} for M = Li; 131.6 kcal mol^{-1} for M = Na; 110.9 kcal mol^{-1} for M = K) and for **2**−M (170.0 kcal mol^{-1} for M = Li; 137.5 kcal mol^{-1} for M = Na; 115.4 kcal mol^{-1} for M = K). These values should be compensated for by a decrease in the solvation energies for the metal ions with increasing size, as exemplified by the calculated solvation energy for $M^+(Me_2O)_4$, which serves as a model for metal ions solvated with four molecules of THF (−122.9 kcal mol^{-1} for M = Li; −94.7 kcal mol^{-1} for M = Na; −67.7 kcal mol^{-1} for M = K). This compensation results in a small difference in the overall energy for dissociation of **1**−M or **2**−M in ethereal solutions, thus supporting the similar $\Delta G^{\ddagger}$ values observed for the intramolecular metal exchange.

Introduction

Cyclopentadienyl (Cp) alkali metal complexes and their derivatives[1,2] are widely used in organic and organometallic syntheses, and therefore the understanding of the reactivity of these complexes based on the nature of metals is important for the effective usage of these complexes. For such purposes, the systematic structural elucidation of Cp−M complexes (M = Li, Na, K) with various structures in solid state is helpful, and extensive structural studies using X-ray crystallography have been carried out.[1−3] So far, several types of solid-state structures of Cp−M derivatives, including the free Cp anion, the monomeric contact ion pair (CIP), the sandwich-type dimer, the oligomer, and the polymer, have been demonstrated to be present for the Cp complexes depending on a variety of substituents and ligands (i.e., solvents or additives such as crown ether, TMEDA, etc.).[1,2]

However, because the synthetic reactions are usually conducted in solution, studies of the structures and dynamic behaviors of Cp−M complexes in solution are especially important to increasing our understanding of the reactivity of these complexes. The variable-temperature NMR technique is one of the common and practical methods for observing such a dynamic process in solution. In 1990, Paquette, Schleyer, and their co-workers reported the first comprehensive study of the

* Corresponding author. E-mail: komatsu@scl.kyoto-u.ac.jp.

(1) Harder, S. *Coord. Chem. Rev.* **1998**, *176*, 17−66. Due to failures from Elsevier publishers, the original article was published with many errors, erratum: *Coord. Chem. Rev.* **2000**, *199*, 331−334. Corrected reprints of the full article are available free of charge upon request from the author.

(2) (a) Jutzi, P.; Burford, N. *Chem. Rev.* **1999**, *99*, 969−990. (b) Jutzi, P.; Reumann, G. *J. Chem. Soc., Dalton Trans.* **2000**, 2237−2244.

(3) Weiss, E. *Angew. Chem., Int. Ed. Engl.* **1993**, *32*, 1501−1523.

10.1021/ja0346431 CCC: $25.00

dynamic behavior of Cp−Li complexes in a THF solution.[4] By means of a dynamic ^{6}Li NMR technique and theoretical calculations, they revealed that the CIP monomer of isodicyclopentadienyllithium is in equilibrium with the sandwich-type dimer and that the equilibrium is shifted to dimer formation at lower temperatures. From these results, they concluded that the change in the aggregation state is responsible for the temperature-dependent exo/endo stereoselectivity in the reaction of isodicyclopentadienyllithium with electrophiles.[4,5] Subsequently, the dynamic behaviors of several derivatives of Cp−Li complexes have been reported on the basis of the variable-temperature ^{6}Li or ^{7}Li NMR technique.[6−8]

In contrast, derivatives of Cp−Na and Cp−K have eluded any dynamic NMR measurements, despite fundamental interest in the dynamic behaviors of these complexes in solution in comparison with that of Cp−Li. One reason for the lack of such measurements is that the resolution of ^{23}Na and ^{39}K NMR is too low to allow precise investigation using line-shape analysis of dynamic NMR spectra. The other is a presumption that dynamic processes of Cp−Na and Cp−K in solution might be too fast to be observed on the NMR time-scale due to the lower binding energies of Na^+ and K^+ with Cp^- than that of Li^+ with Cp^-.

As a part of our continued studies of the synthesis and properties of a series of cyclic π-conjugated systems annelated with bicyclo[2.2.2]octene (abbreviated as BCO),[9,10] we became interested in a cyclopentadienyl system.[1−2,11−12] Annelation of a planar π-system with BCO units is advantageous in that one face of the π-system, on which a chemical event takes place, can be distinguished from the other by observing the ^{13}C NMR signals for the methylene carbons of the BCO unit, which are differentiated from those on the other side of the π-system. By using this technique, we have previously determined the kinetics of dynamic intra- and intermolecular proton migration in a protonated, Wheland-type σ-complex of tris-BCO-annelated benzene.[10b] The same technique is expected to be applicable to the Cp−M complex annelated with BCO units, if the rate for site exchange of the complexed metal ion, shown by Scheme 1, is measurable on the NMR time-scale. This method is particularly advantageous in that it is applicable regardless of the type of metal ion. We report herein the results of first systematic study of the dynamic behavior of a series of cyclopentadienyl-alkali metal derivatives, i.e., **1**−M and **2**−M (M = Li, Na, K). The results will be also discussed together with the crystal structures obtained by X-ray crystallography and the results of theoretical calculations.

Scheme 1

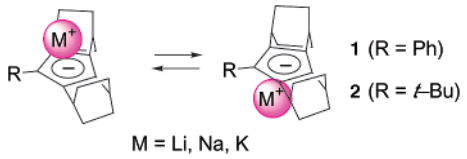

Scheme 2

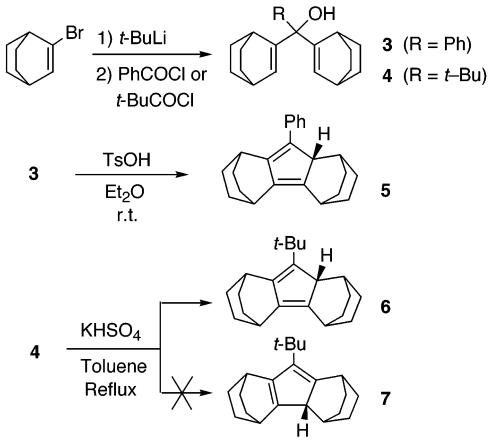

Results and Discussion

Synthesis. Syntheses of cyclopentadiene derivatives annelated with bicyclo[2.2.2]octene (BCO) units, **5** and **6**, were conducted as shown in Scheme 2. Addition of 0.5 equiv of benzoyl chloride or pivaloyl chloride to 2-lithiobicyclo[2.2.2]octene, generated from 2-bromobicyclo[2.2.2]octene with *tert*-butyllithium, gave 3-phenyl- or 3-*tert*-butyl-1,4-pentadien-3-ol derivatives **3** or **4**, respectively. The acid-catalyzed electrocyclization of **3** with *p*-toluenesulfonic acid[13] and **4** with potassium hydrogenesulfate[14] using the Dean−Stark apparatus afforded phenylcyclopentadiene **5** in 56% and *tert*-butylcyclopentadiene **6** in 34% isolated yield after chromatographic purification on alumina.

Of the three conceivable double-bond isomers of the cyclopentadiene system, only one isomer with a cyclopentadienyl proton attached to an asymmetric position was obtained for both the phenyl and *tert*-butyl derivatives. For the phenyl derivative **5**, the structure was unambiguously determined by X-ray crystallography (Figure 1), while the structure of the *tert*-butyl derivative was deduced based on the results of theoretical calculations, as follows. Upon comparison of the total energy (B3LYP/6-31G(d)), the isomer **6** was calculated to be more stable than **7** by 2.1 kcal mol^{-1}, and also the observed NMR chemical shifts for the sp^2 carbons (δ 145.0, 142.7, 140.9, 139.5) were found to be much closer to the calculated chemical shifts (GIAO/HF/6-31+G(d,p)//B3LYP/6-31G(d)) for **6** (δ 144.0, 141.2, 140.7, 139.0) than to those for **7** (δ 151.6, 149.1, 148.0, 141.6).

(4) Paquette, L. A.; Bauer, W.; Sivik, M. R.; Bühl, M.; Feigel, M.; Schleyer, P. v. R. *J. Am. Chem. Soc.* **1990**, *112*, 8776−8789.
(5) Zaegel, F.; Gallucci, J. C.; Meunier, P.; Gautheron, B.; Sivik, M. R.; Paquette, L. A. *J. Am. Chem. Soc.* **1994**, *116*, 6466−6467.
(6) (a) Bauer, W.; O'Doherty, G. A.; Schleyer, P. v. R.; Paquette, L. A. *J. Am. Chem. Soc.* **1991**, *113*, 7093−7100. (b) Bauer, W.; Sivik, M. R.; Friedrich, D.; Schleyer, P. v. R.; Paquette, L. A. *Organometallics* **1992**, *11*, 4178−4189. (c) Paquette, L. A.; Sivik, M. R.; Bauer, W.; Schleyer, P. v. R. *Organometallics* **1994**, *13*, 4919−4927. (d) Sivik, M. R.; Bauer, W.; Schleyer, P. v. R.; Paquette, L. A. *Organometallics* **1996**, *15*, 5202−5208.
(7) Eiermann, M.; Hafner, K. *J. Am. Chem. Soc.* **1992**, *114*, 135−140.
(8) (a) Kunz, K.; Pflug, J.; Bertuleit, A.; Fröhlich, R.; Wegelius, E.; Erker, G.; Würthwein, E.-U. *Organometallics* **2000**, *19*, 4208−4216. (b) Kunz, K.; Erker, G.; Kehr, G.; Fröhlich, R. *Organometallics* **2001**, *20*, 392−400.
(9) Komatsu, K. *Bull. Chem. Soc. Jpn.* **2001**, *74*, 407−419.
(10) (a) Komatsu, K.; Akamatsu, H.; Jinbu, Y.; Okamoto, K. *J. Am. Chem. Soc.* **1988**, *110*, 633−634. (b) Komatsu, K.; Aonuma, S.; Jinbu, Y.; Tsuji, R.; Hirosawa, C.; Takeuchi, K. *J. Org. Chem.* **1991**, *56*, 195−203. (c) Nishinaga, T.; Komatsu, K.; Sugita, N.; Lindner, H. J.; Richter, J. *J. Am. Chem. Soc.* **1993**, *115*, 11642−11643. (d) Nishinaga, T.; Izukawa, Y.; Komatsu, K. *J. Am. Chem. Soc.* **2000**, *122*, 9312−9313. (e) Matsuura, A.; Nishinaga, T.; Komatsu, K. *J. Am. Chem. Soc.* **2000**, *122*, 10007−10016. (f) Wakamiya, A.; Nishinaga, T.; Komatsu, K. *Chem. Commun.* **2002**, 1192−1193. (g) Nishinaga, T.; Inoue, R.; Matsuura, A.; Komatsu, K. *Org. Lett.* **2002**, *4*, 4117−4120. (h) Wakamiya, A.; Nishinaga, T.; Komatsu, K. *J. Am. Chem. Soc.* **2002**, *124*, 15038−15050.
(11) (a) Breslow, R.; Hill, R.; Wasserman, E. *J. Am. Chem. Soc.* **1964**, *86*, 5349−5350. (b) Saunders: M.; Berger, R.; Jaffe, A.; McBride, J. M.; O'Neil, J.; Breslow, R.; Hoffman, J. M., Jr.; Perchonock, C.; Wasserman, E.; Hutton, R. S.; Kuck, V. J. *J. Am. Chem. Soc.* **1973**, *95*, 3017−3018.
(12) Sitzmann, H.; Bock, H.; Boese, R.; Dezember, T.; Havlas, Z.; Kaim, W.; Moscherosch, M.; Zanathy, L. *J. Am. Chem. Soc.* **1993**, *115*, 12003−12009.
(13) Threlkel, R. S.; Bercaw, J. E. *J. Organomet. Chem.* **1977**, *136*, 1−5.
(14) Erker, G.; van der Zeijden, A. A. H. *Angew. Chem., Int. Ed. Engl.* **1990**, *29*, 512−514.

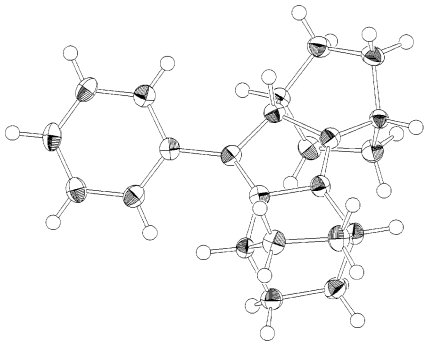

Figure 1. ORTEP drawing (50% probability) of the molecular structure of **5**.

Scheme 3

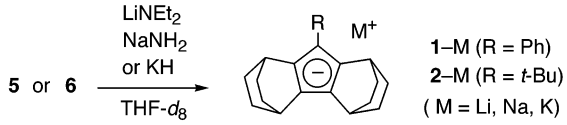

The rather modest isolation yields of **5** and **6** are attributed to inevitable partial decomposition during the purification process, since the yield of both **5** and **6** estimated from the ^{1}H NMR spectra of the crude products was more than 80%.

By the use of ethyl formate in the first step of Scheme 2 followed by acid-catalyzed cyclization using potassium hydrogenesulfate, the BCO-annelated cyclopentadiene having no additional substituent was produced. Unfortunately, however, the extreme lability of this compound hampered its isolation. Also, the attempted synthesis of the methyl derivative was not successful due to the possible deprotonation of the methyl group in the course of the acid-catalyzed cyclization of the 3-methylpentadienol derivative.

As to the preparation of Cp−Li complexes, *n*-BuLi or MeLi is commonly used for the deprotonation of cyclopentadienes. However, in the case of the reactions of **5** and **6**, 1 equiv of either of these reagents was not sufficient to complete the reaction in THF. Formation of the lithium complex of *tert*-butyl and phenyl derivatives **1**−Li and **2**−Li was so slow that some of the reagent seemed to be consumed by a side reaction possibly occurring with the solvent, THF. Thus, lithium diethylamide was chosen, and the formation of **1**−Li and **2**−Li proceeded quite smoothly in THF. For the sodium and potassium complexes, the use of 1 equiv of sodium amide and potassium hydride, respectively, was found to be suitable for the deprotonation of **5** and **6** in THF (Scheme 3). In all of these reactions, the formation of **2** was generally much slower than that of **1**. For example, heating at 50 °C for 2 h was required for the formation of **2**−Li, while the formation of **1**−Li was completed at room temperature within a few minutes. Also, sonication at room temperature for 24 h was required for the formation of **2**−Na, while sonication for 1 h was sufficient for **1**−Na. In the case of the formation of potassium complexes, the reaction was completed within a few minutes after mixing the Cp derivatives with 1 equiv of potassium hydride for both **5** and **6**.

Structures of Cp−M Complexes. Among the six Cp−M derivatives **1**−M and **2**−M (M = Li, Na, K), single crystals were obtained for **1**−Li, **1**−Na, and **2**−Na from their THF solutions that were sealed under vacuum and kept in a freezer (−20 °C) for 4 to 6 days. The precise structures of these complexes were determined by X-ray crystallography. As shown in Figure 2, all of these three complexes formed monomeric contact ion pairs (CIPs) with two to three THF molecules coordinated to the metal ion. In general, the solid-state structure of Cp−alkali metal complexes, crystallized from nonpolar solvents, is known to be composed of one-dimensional polymeric chains with super-sandwich structures of alternating Cp anions and metal cations.[1,15−17] These polymeric chains of the

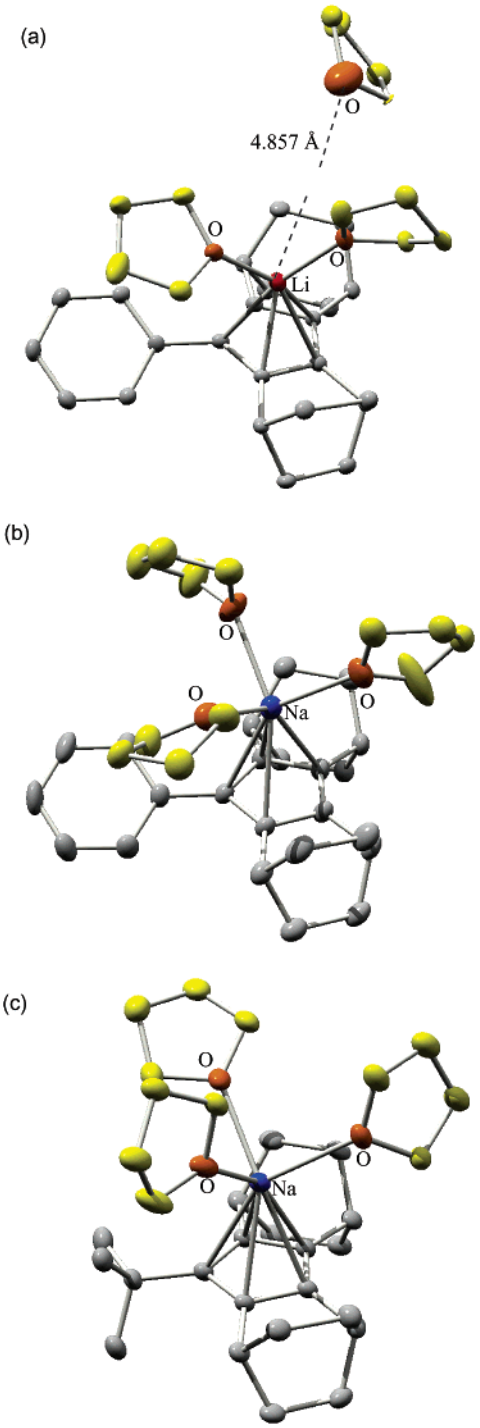

Figure 2. Thermal ellipsoid (50% probability) drawings showing X-ray structures of (a) **1**−Li(THF)$_2$(THF), (b) **1**−Na(THF)$_3$, and (c) **2**−Na(THF)$_3$. Hydrogen atoms are omitted.

(15) Jutzi, P.; Leffers, W.; Hampel, B.; Pohl, S.; Saak, W. *Angew. Chem., Int. Ed. Engl.* **1987**, *26*, 583−584.
(16) Evans, W. J.; Boyle, T. J.; Ziller, J. W. *Organometallics* **1992**, *11*, 3903−3907.

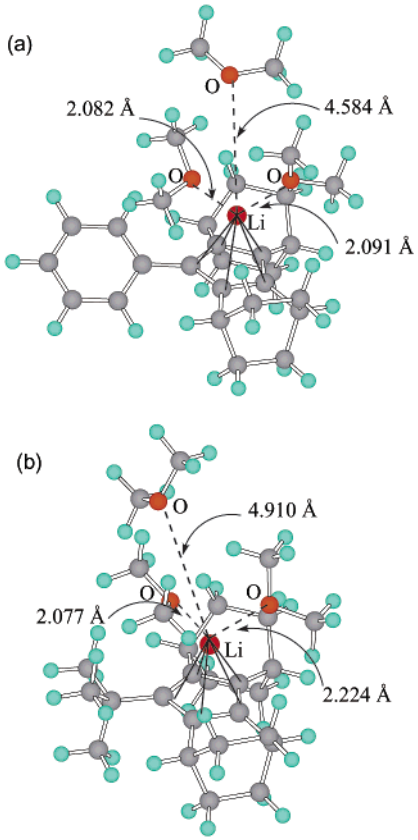

Figure 3. The optimized structures of (a) **1**−Li(Me_2O)$_3$ and (b) **2**−Li(Me_2O)$_3$ at the B3LYP/6-31G(d) level.

Li complexes are broken up into monomers even in moderately polar solvents such as THF, while partly solvated polymeric chains are still formed in most single crystals of Na and K complexes obtained from THF.[1] Only one example of the K salt of a pentabenzyl Cp derivative crystallized from a THF solution has been reported to form a monomeric CIP in the solid state.[18] In this case, the 5-fold substitution with such bulky groups on the Cp ring is considered to have prevented the formation of polymer chains. For the same reason, the Na complexes of **1** and **2**, as well as the Li complex of **1**, are supposed to form monomeric CIPs rather than solvated polymeric chains.

The number of THF molecules directly coordinated to Li^+ ion in **1** was shown to be two, while that in **1**−Na and **2**−Na was three. In the **1**−Li complex, the third THF molecule is located in a remote position with a Li−O distance of 4.857 Å. This difference in the mode of coordination is attributed to the difference in both the C_{Cp}−M and M−O distances. The distances of C_{Cp}−Li and Li−O in the **1**−Li complex involving two directly coordinated THF molecules (averaged values, 2.288 and 1.997 Å, respectively) are considerably shorter than those of C_{Cp}−Na and Na−O in the **2**−Na complex (averaged values, 2.760 and 2.377 Å, respectively), and hence these two tightly coordinated THF molecules in **1**−Li must prevent the direct coordination of the third THF molecule. In this connection, it should be noted that the X-ray structure of 1,2,4-(Me_3Si)$_3$Cp−Li crystallized from THF, in which the Cp anion is kinetically and electronically stabilized by three trimethylsilyl substituents, showed that only one THF molecule can be coordinated to the Li^+ ion.[19]

In support of the above interpretation, according to the theoretical calculations (B3LYP/6-31G(d)) conducted for **1**−Li(Me_2O)$_3$ and **2**−Li(Me_2O)$_3$ using dimethyl ether as a model ligand in place of THF for simplification of the calculations (Figure 3), only two molecules of the Me_2O ligand are directly coordinated to Li^+, while another one is separated with a Li−O distance of 4.584 Å for **1** and 4.910 Å for **2**. This long Li−O distance calculated for **1**−Li(Me_2O)$_3$ is in reasonably good agreement with the observed value for **1**−Li(THF)$_2$(THF) (see above). This result also indicates that the present calculation using Me_2O as a model ligand is valid for the examination of structural features and probably for the estimation of the stabilization energies occurring with ligand coordination as well. Hence, we used Me_2O as a model of THF for all the theoretical calculations in the present study.

Despite the long Li−O distance observed between the third THF molecule and **1**−Li, some stabilizing interaction between the separated THF molecule and Li^+ ion seems to be present, judging from the energy differences between **1**(or **2**)−Li, **1**(or **2**)−Li(Me_2O)$_2$, and **1** (or **2**)−Li(Me_2O)$_3$ obtained by theoretical calculations (B3LYP/6-31G(d)), as described below.

The stabilization energy by ligand coordination was calculated for equations (1) to (4). It is clearly shown that considerable stabilization energies are obtained with the coordination of two Me_2O molecules to both **1**−Li and **2**−Li (eqs 1 and 2):

$$\mathbf{1}\text{−Li} + 2\ (Me_2O) \rightarrow \mathbf{1}\text{−Li}(Me_2O)_2$$

$$\Delta E_1 = -27.7\ \text{kcal mol}^{-1} \qquad (1)$$

$$\mathbf{2}\text{−Li} + 2\ (Me_2O) \rightarrow \mathbf{2}\text{−Li}(Me_2O)_2$$

$$\Delta E_2 = -23.2\ \text{kcal mol}^{-1} \qquad (2)$$

Furthermore, some additional stabilization energy was found to result from coordination of the third ligand, despite the longer Li−O distance (eqs 3 and 4):

$$\mathbf{1}\text{−Li}(Me_2O)_2 + (Me_2O) \rightarrow \mathbf{1}\text{−Li}(Me_2O)_3$$

$$\Delta E_3 = -2.9\ \text{kcal mol}^{-1} \qquad (3)$$

$$\mathbf{2}\text{−Li}(Me_2O)_2 + (Me_2O) \rightarrow \mathbf{2}\text{−Li}(Me_2O)_3$$

$$\Delta E_4 = -2.6\ \text{kcal mol}^{-1} \qquad (4)$$

Another notable structural feature of these complexes is the distances between each carbon of the Cp ring (C_{Cp}) and the metal ion. The averaged values of observed C_{Cp}−M distances are listed in Table 1 together with those obtained by theoretical calculations (B3LYP/6-31G(d)). It is known that the C_{Cp}−M distance is influenced both by the substituents on the Cp ring and by the type and number of ligands. In general, electron-releasing substituents destabilize the Cp anion and hence shorten the C_{Cp}−M distances, thus reducing polarization of the C_{Cp}−M bonds; in contrast, increasing the number of ligands on the metal causes an elongation of C_{Cp}−M distances.[1] Upon comparison

(17) Dinnebier, R. E.; Behrens, U.; Olbrich, F. *Organometallics* **1997**, *16*, 3855−3858.
(18) Lorberth, J.; Shin, S.-H.; Wocadlo, S.; Massa, W. *Angew. Chem., Int. Ed. Engl.* **1989**, *28*, 735−736.
(19) Jutzi, P.; Leffers, W.; Pohl, S.; Saak, W. *Chem. Ber.* **1989**, *122*, 1449−1456

Table 1. Averaged C_{Cp}−M and M−O Distances of **1**−M(ligand)$_n$ and **2**−M(ligand)$_n$

compd	method	number of ligand[a] (n)	C_{Cp}–M (Å)	M–O (Å)
1−Li	X-ray	2(+1)	2.288	1.997 (4.857)
	calcd[b]	0	2.113	−
	calcd[b]	2(+1)	2.270	2.088 (4.584)
1−Na	X-ray	3	2.760	2.377
	calcd[b]	0	2.527	−
	calcd[b]	3	2.707	2.429
1−K	calcd[b]	0	2.908	−
	calcd[b]	3	3.028	2.773
2−Li	calcd[b]	0	2.105	−
	calcd[b]	2(+1)	2.264	2.151 (4.910)
2−Na	X-ray	3	2.720	2.413
	calcd[b]	0	2.521	−
	calcd[b]	3	2.699	2.499
2−K	calcd[b]	0	2.897	−
	calcd[b]	3	3.008	2.836

[a] The ligand for the X-ray analysis was THF while dimethyl ether was used as a model ligand for calculations. [b]B3LYP/6-31G(d).

of the observed structures of Na complexes, **1**−Na(THF)$_3$ and **2**−Na(THF)$_3$, the averaged length of C_{Cp}−M bonds for the derivative with the electron-releasing *tert*-butyl group was found to be shorter than that in the phenyl derivative by 0.04 Å, as expected. Furthermore, the theoretical calculations indicated shorter C_{Cp}−M distances for **2**−M in comparison with **1**−M, irrespective of the absence or presence of the ligand. Thus, a *tert*-butyl substituent of the Cp ring causes formation of a tighter Cp−M complex than does a phenyl substituent, although the effect is not large. Elongation of the Cp−M distance upon increases in the number of ligand was also supported by the calculations.

In contrast to the C_{Cp}−M distance, the averaged distance between the metal ion and oxygen atom of the ligand, the M−O distance, showed a reversed tendency. Thus, the observed M−O distance in **2**−Na(THF)$_3$ was longer than that in **1**−Na(THF)$_3$ (Table 1), and the same tendency was also found in the calculated structures for other **1**−M(Me$_2$O)$_3$ and **2**−M(Me$_2$O)$_3$ complexes. This increase is again ascribed to the substituent effect on the charge of the Cp ring. As mentioned above, the *tert*-butyl substituent suppresses the polarization between the Cp moiety and the metal. As a result, the less positively charged metal in **2**−M, as compared with **1**−M, would lengthen the M−O distance. To more accurately estimate the metal's charge,[20] natural population analysis was performed. As shown in Table 2, the aforementioned presumption is supported by the comparison of the calculated charge distribution of **1**−M and **2**−M both in the absence and presence of the Me$_2$O ligand. The metal ion's charge in **2**−M was found to be slightly lower than that in **1**−M both in the absence and presence of the ligand.

Dynamic Behavior. The Cp−Li Complexes. First, the dynamic behavior of the BCO-annelated cyclopentadienyllithium complexes having phenyl and *tert*-butyl groups (**1**−Li and **2**−Li) was investigated by the variable-temperature NMR technique. In the ^{13}C NMR spectrum of **2**−Li in THF-d_8 at 30 °C, the signals for the methylene carbons in the BCO units (marked with ○ and Δ) showed four signals at 31.5, 30.8, 30.2, and 29.8 ppm, while the signals for the bridgehead carbons (marked with ●) showed only two signals (Figure 4b). This

Table 2. Calculated Charge Distribution Obtained as Natural Charge[a] for **1**−M(Me$_2$O)$_n$ and **2**−M(Me$_2$O)$_n$

compd	number of Me$_2$O (n)	charge density M	charge density (Me$_2$O)$_3$
1−Li	0	0.925	−
	3	0.894	0.041
1−Na	0	0.936	−
	3	0.901	0.040
1−K	0	0.954	−
	3	0.913	0.041
2−Li	0	0.918	−
	3	0.892	0.038
2−Na	0	0.931	−
	3	0.897	0.040
2−K	0	0.951	−
	3	0.907	0.043

[a] Obtained by natural population analysis (B3LYP/6-31G(d)).

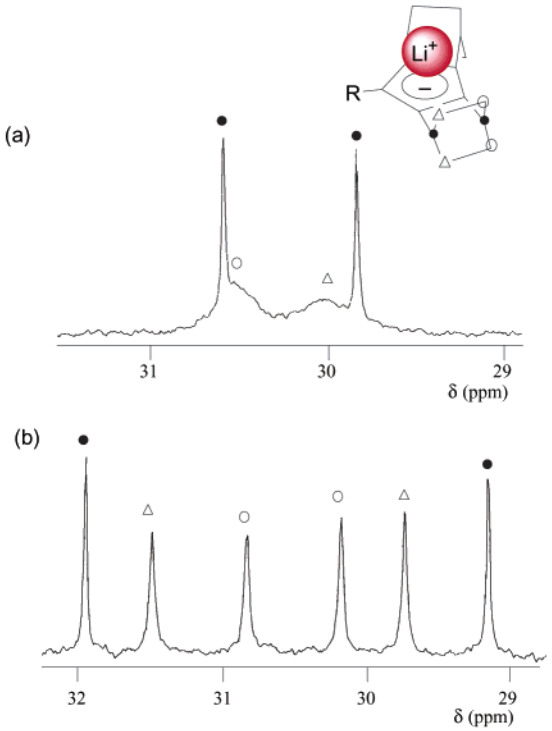

Figure 4. The expanded ^{13}C NMR for (a) **1**−Li and (b) **2**−Li at 30 °C in THF-d_8. [**1**−Li] = [**2**−Li] = 0.2 M. The signals marked with ○ and Δ correspond to methylene cabons, and that marked with ● corresponds to bridgehead carbons of the BCO units.

indicates that the environments of the upper and lower faces of the Cp ring of **2** are nonequivalent under these conditions, most probably due to the static coordination with the Li$^+$ ion on one face. In contrast, the methylene carbons of **1**−Li (marked with ○ and Δ) were observed as two broad signals at 30.6 and 30.0 ppm (Figure 4a) under the same conditions, while the signals for the bridgehead carbons (marked with ●) remained as two sharp signals. As shown in Figure 5a, these two broad signals were split into four signals at a lower temperature (−60 °C). This clearly indicates that the dynamic behavior in the **1**−Li complex shown in Scheme 1, which is fast at 30 °C, becomes slow to make the upper- and lower-face methylene signals distinguishable on the NMR time-scale at lower temperatures. During the variable-temperature measurements, no apparent change was observed for other signals, i.e., those for Cp-ring carbons (δ 118.3, 118.0, 108.3) and bridgehead carbons (δ 30.6, 29.8).

(20) Lamberet, C.; Schleyer, P. v. R. *Angew. Chem., Int. Ed. Engl.* **1994**, *33*, 1129−1140.

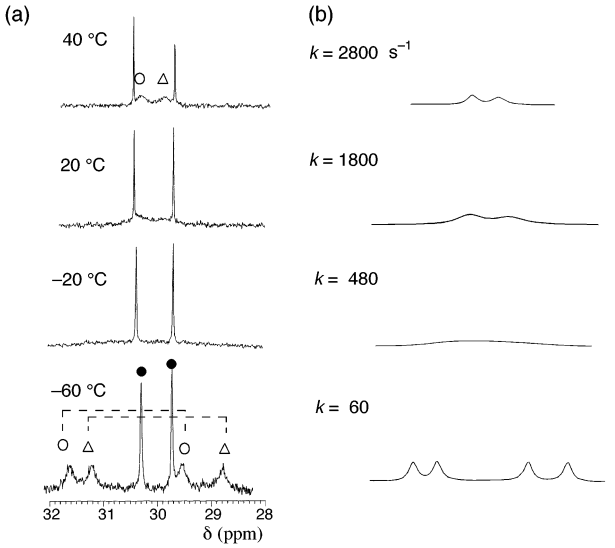

Figure 5. Temperature-dependent (a) experimental and (b) simulated ^{13}C NMR spectra of **1**−Li in THF-d_8. The signals marked with ○ and Δ correspond to methylene cabons, and that marked with ● corresponds to bridgehead carbons of the BCO units. [**1**−Li] = 0.1 M.

On the other hand, in the ^{7}Li NMR only a sharp signal was observed at −7.34 ppm for **1**−Li and at −8.60 ppm for **2**−Li at room temperature, and no broadening was observed upon cooling to −90 °C. The observed ^{7}Li NMR chemical shifts are comparable to previously reported values for monomeric CIP of cyclopentadienyllithium (−8.60 ppm) and isodicyclopentadienyllithium (−8.30 ppm) in THF-d_8,[4] suggesting that **1**−Li and **2**−Li are also present as monomeric CIPs in THF both at 30 °C and at −90 °C in the ground state. The sandwich-type dimer, which had been observed in other Cp−lithium derivatives,[4,6−8] was not detected in the low-temperature ^{7}Li and ^{13}C NMR measurements of **1**−Li and **2**−Li.

The rate of dynamic process showed no detectable dependence on **1**−Li in concentrations at a range from 0.05 to 0.2 M, suggesting that the site exchange of the Li^+ ion in **1**−Li proceeds dominantly as an intramolecular process. Therefore, the observed rate constant (k) obtained by line-shape analysis (Figure 5) would be approximately equal to the rate constant of the internal exchange (k_1, s^{-1}; the inset of Figure 6).[21] The thermodynamic parameters (25 °C) of the dynamic process in **1**−Li obtained by the line-shape analysis and Arrhenius plot (Figure 6) are: $\Delta H^{\ddagger} = 4.6 \pm 0.4$ kcal mol^{-1} and $\Delta S^{\ddagger} = -27 \pm 2$ eu (Table 3). The large negative value of $\Delta S^{\ddagger}$ indicates that a highly ordered molecular assembly is involved in the transition state of the Li^+ exchange. However, any aggregation of **1**−Li in the transition state is unlikely because no concentration-dependence was observed for k_1.[21] Rather, the transition state is considered to involve an assembly of solvent molecules, probably due to the formation of a solvent-separated ion pair (SSIP), although the ground-state structure of **1**−Li is a CIP. Normally, a solvated Li^+-ion assembly in THF consists of four

(21) One referee suggested that this dynamic process might involve an associative mechanism where a Li^+ ion adds to **1**−Li to form an inverse sandwich cation that then decomposes by subsequent Li^+ dissociation. However, such mechanism can be ruled out from the following reasons. First, no rate dependence on the concentration of **1**−Li was observed at all for this process. Second, the concentration of a free Li^+ ion that could participate in the formation of such an inverse sandwich cation should be quite low in the absence of added Li salt, as judged from the ^{7}Li NMR measurements, and furthermore, the overall k value was found to be not so sensitive to the concentration of added Li salts.

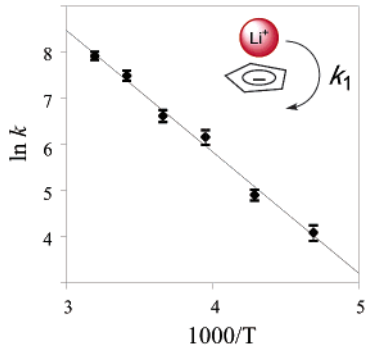

Figure 6. Arrhenius plot of the kinetic data obtained by the line-shape analysis (Figure 5) for **1**−Li in THF-d_8.

Table 3. Thermodynamic Parameters (25 °C) for the Dynamic Processes of **1**−M and **2**−M in THF-d_8

compd	type of k	$\Delta H^{\ddagger}$ (kcal mol^{-1})	$\Delta S^{\ddagger}$ (eu)	$\Delta G^{\ddagger}$ (kcal mol^{-1})
1−Li	k_1[a]	4.6 ± 0.4	−27 ± 2	12.6 ± 0.1
	k_1(+LiBr)[b]	4.4 ± 1.3	−29 ± 6	13.0 ± 0.3
	k'(+LiBr)[c]	5.5 ± 0.9	−21 ± 4	11.7 ± 0.2
1−Na	k_1[a]	0.8 ± 0.4	−38 ± 2	12.1 ± 0.2
1−K	k_1[a]	1.5 ± 1.3	−35 ± 6	12.0 ± 0.4
2−Li	k'(+LiBr)[d]	7.0 ± 2.3	−25 ± 7	14.5 ± 0.1
2−Na	k_1[a]	0.4 ± 1.4	−45 ± 7	13.7 ± 0.7
	k_2[e]	0.7 ± 0.7	−37 ± 4	11.9 ± 0.4
2−K	k_1[a]	5.2 ± 1.1	−25 ± 5	12.7 ± 0.5
	k_2[e]	6.8 ± 0.8	−13 ± 3	10.7 ± 0.2

[a] For intramolecular exchange. [b] For intramolecular exchange in the presence of added LiBr; obtained from eq 5. [c] For external exchange with LiBr; obtained from eq 5. [d] For external exchange; obtained from eq 6. [e] For intermolecular exchange; obtained from eq 7.

solvent molecules per Li^+ ion,[4] whereas only two THF molecules are directly bound to Li^+ ion in the solid state of **1**−Li (Figure 2a). Therefore, at least two additional THF molecules are supposed to lose a degree of freedom in the formation of SSIP if we assume that the ground-state structure is similar to that in the solid-state. In addition, the charge on the Cp ring in CIP that was calculated to be −0.935 is considered to become more negative upon separation of the cation (upon formation of SSIP), and greater solvation should be required for the more negatively charged Cp ring. These suppositions are all in agreement with the highly negative value of $\Delta S^{\ddagger}$.

In contrast, the intramolecular Li^+ exchange in **2**−Li was too slow in THF at 30 °C to be observed on the NMR timescale. This is ascribed partly to the electronic effect of the *tert*-butyl substituent that makes the Cp−Li bonds stronger as described above. This hypothesis is in agreement with the results of a comparison of the calculated dissociation energy (B3LYP/6-31G(d)) of the solvent-coordinated CIPs shown in eq 11 and Table 8 (see below).[22] Thus, the dissociation of **2**−Li(Me_2O)$_3$ (+72.7 kcal mol^{-1}; Table 8) was calculated to be more endothermic than that of **1**−Li(Me_2O)$_3$ (+70.3 kcal mol^{-1}; Table 8) by 2.4 kcal mol^{-1}.

Although *tert*-butyl derivative **2**−Li did not exhibit any intramolecular dynamic behavior in the ^{13}C NMR spectrum at

(22) The values of dissociation energies shown in Table 4 are much larger than the observed values of $\Delta H^{\ddagger}$ because any stabilizing interaction between the Cp^- anion and $Li^+(Me_2O)_4$ and also the solvation energy of the Cp^- anion are neglected. With respect to the importance of the former interaction, MNDO calculations have shown that the stabilization energy for the interaction between isodicyclopentadienide ion and $Li^+(H_2O)_4$ in SSIP would be −58.6 kcal mol^{-1} in a previous study by Paquette et al.[4]

Table 4. Kinetic Data for Internal and External Metal Exchange for **1**−Li in the Absence and Presence of Added LiBr

temp (°C)	k_1^a (s^{-1})	k_1^b (s^{-1})	k'^b (L mol^{-1} s^{-1})
40	2800 ± 300	–	–
20	1800 ± 200	1500 ± 500	16800 ± 3000
0	750 ± 100	780 ± 260	6600 ± 1300
−20	480 ± 75	470 ± 190	2100 ± 780
−40	140 ± 15	140 ± 56	980 ± 270
−60	60 ± 10	60 ± 17	310 ± 86

[a] Values obtained in the absence of LiBr. [b]Values obtained from eq 5 in the presence of added LiBr.

Table 5. Kinetic Data for External Metal Exchange for **2**−Li Obtained from Eq 6

temp (°C)	k' (L mol^{-1} s^{-1})
60	560 ± 140
50	370 ± 86
40	280 ± 62
30	170 ± 46
10	66 ± 23
0	47 ± 15

Table 6. Kinetic Data for the Metal-Ion Site Exchange of **1**−Na and **2**−Na in THF

temp (°C)	$k_{1(1-Na)}$ (s^{-1})	$k_{1(2-Na)}^a$ (s^{-1})	$k_{2(2-Na)}^a$ (L mol^{-1} s^{-1})
−20	5800 ± 600	460 ± 220	7600 ± 1900
−40	4100 ± 460	360 ± 160	5700 ± 1300
−60	3100 ± 450	310 ± 140	4900 ± 1100
−80	2400 ± 310	260 ± 100	3700 ± 730
−100	1500 ± 260	174 ± 100	2100 ± 780

[a] Values obtained from eq 7 (M = Na).

Table 7. Kinetic Data for the Metal-Ion Site Exchange of **1**−K and **2**−K in THF

temp (°C)	$k_{1(1-K)}$ (s^{-1})	$k_{1(2-K)}^a$ (s^{-1})	$k_{2(2-K)}^a$ (L mol^{-1} s^{-1})
0	–	1500 ± 580	22500 ± 5000
−20	5300 ± 1200	430 ± 150	10500 ± 1500
−40	3300 ± 1200	170±750	4000 ± 750
−60	2500 ± 770	45 ± 12	600 ± 100
−80	1400 ± 770	18 ± 4	88 ± 33
−100	750 ± 390	–	–

[a] Values obtained from eq 7 (M = K).

Table 8. Calculated Dissociation Energy for Cp−M (ΔE_{11} in Eq 11) and Calculated Energy for Formation of $(Cp-M-Cp)^-$ (ΔE_{12} in Eq 12)

Cp–M	ΔE_{11} (kcal mol^{-1})	ΔE_{12} (kcal mol^{-1})
1−Li	+70.3	+69.2
1−Na	+73.9	+71.0
1−K	+75.1	+69.8
2−Li	+72.7	+70.7
2−Na	+75.8	+69.5
2−K	+78.2	+69.7

30 °C (Figure 4b), when LiBr was added to **2**−Li in THF-d_8, an intermolecular Li^+ exchange could be observed, as shown in Figure 7. The exchange rate was independent of the concentration of **2**−Li in the range from 0.1 to 0.2 M, but increased in proportion to the concentration of the added LiBr in the range from 0.1 to 0.4 M (Figure 8a).

Also in the case of phenyl derivative **1**−Li, a similar rate-acceleration was observed when LiBr was added. The observed rate (k) was again independent of the concentration of **1**−Li in the concentration range from 0.05 to 0.2 M but increased in proportion to the concentration of LiBr in the range from 0.05

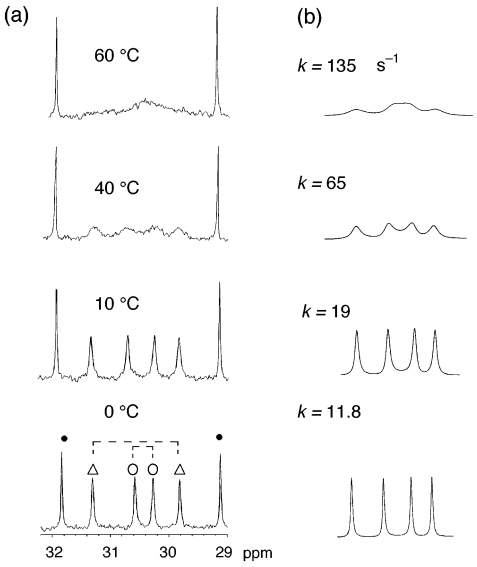

Figure 7. Temperature-dependent (a) experimental and (b) simulated ^{13}C NMR spectra of **2**−Li in THF-d_8 in the presence of 0.2 M LiBr. The signals marked with ○ and Δ correspond to methylene cabons, and that marked with ● corresponds to bridgehead carbons of the BCO units. [**2**−Li] = 0.2 M.

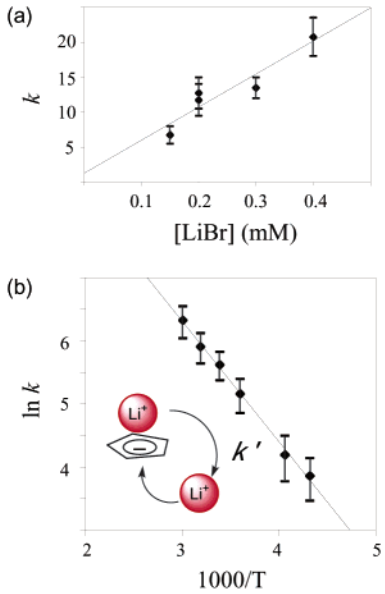

Figure 8. (a) The rate k vs [LiBr] plot (T = 278 K) and (b) Arrhenius plot of the kinetic data obtained by the line-shape analysis (Figure 7) for **2**−Li in THF-d_8 in the presence of added LiBr.

to 0.4 M (Figure 9a). Accordingly, the rate for the exchange with external Li^+ ion (k', L mol^{-1} s^{-1}) can be expressed as the inclination in the plot of the k value against the concentration of LiBr in eqs 5 and 6, and was actually determined at the temperature range from 0 to 60 °C for **2**−Li and from −60 to 20 °C for **1**−Li. The results are shown in Tables 4 and 5

$$k_{(\mathbf{1}-\mathrm{Li})} = k_{1(\mathbf{1}-\mathrm{Li})} + k'_{(\mathbf{1}-\mathrm{Li})}[\mathrm{LiBr}] \quad (5)$$

$$k_{(\mathbf{2}-\mathrm{Li})} = k'_{(\mathbf{2}-\mathrm{Li})}[\mathrm{LiBr}] \quad (6)$$

The activation parameters for the internal and external Li^+ exchange processes obtained from the Arrhenius plots (Figures 8 and 9) using $k_{1(\mathbf{1}-\mathrm{Li})}$ and $k'_{(\mathbf{1}-\mathrm{Li})}$, determined by eq 5, and using $k'_{(\mathbf{2}-\mathrm{Li})}$, determined by eq 6, are also shown in Table 3. The

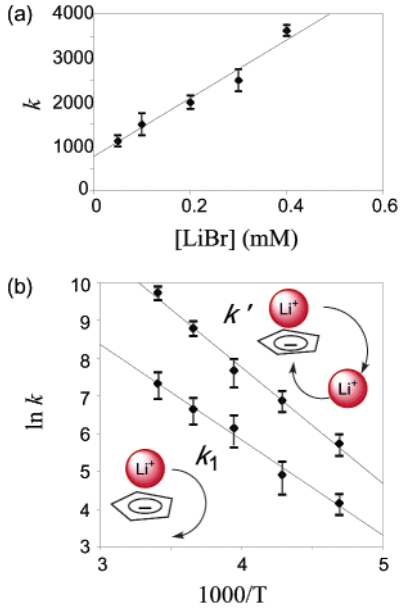

Figure 9. (a) The rate k vs [LiBr] plot (T = 278 K) and (b) Arrhenius plot of the kinetic data obtained by the line-shape analysis for **1**−Li in THF-d_8 in the presence of added LiBr.

$\Delta H^{\ddagger}$ and $\Delta S^{\ddagger}$ values obtained from $k_{1(\mathbf{1}-\mathrm{Li})}$ using eq 5 were in agreement, within the experimental error, with those obtained from $k_{1(\mathbf{1}-\mathrm{Li})}$ in the absence of external LiBr, supporting the validity of the present treatment of the kinetic data according to eq 5. Upon comparison of the activation parameters obtained based on the internal (k_1) and external (k') exchange rates of **1**−Li, we notice that very large negative values of $\Delta S^{\ddagger}$ are observed for both cases and that the values of $\Delta H^{\ddagger}$ and $\Delta G^{\ddagger}$ are rather similar. These results may suggest that the transition states for the both internal and external exchanges involve a similar dissociation process of the Cp−Li bonds, which is accompanied by the high degree of solvation of the ionic species. In this respect, the larger $\Delta H^{\ddagger}$ obtained for **2**−Li (7.0 ± 2.3 kcal mol^{-1}) than that for **1**−Li (5.5 ± 0.9 kcal mol^{-1}) is apparently consistent with the larger calculated dissociation energy of ΔE in eq 11 for **2**−Li than that for **1**−Li, as shown in Table 8 (see below).

The Cp−Na and Cp−K Complexes. For sodium and potassium complexes of **1** and **2**, dynamic site exchange behavior of the metal ion similar to that in **1**−Li was observed upon variable-temperature ^{13}C NMR measurements at a temperature range from 20 to −100 °C. The observed ^{13}C NMR spectra and the results of line-shape analysis for the *tert*-butyl-substituted derivatives **2**−Na and **2**−K are shown in Figures 10 and 12 (see the Supporting Information for the line-shape analysis of **1**−Na and **1**−K). In the spectra of **2**−K (Figure 12a), the split signals for the methylene carbons were observed at −100 °C, while the splitting was not complete for **1**−Na, **1**−K, and **2**−Na in THF, even at −100 °C. However, when a 1:1 mixture of THF-d_8 and toluene-d_8 was used as solvent, the intramoleculer site exchange was found to slow, and the methylene carbons could be observed as split signals. This splitting of the methylene signals implies that CIPs are formed in the ground state for the Na and K complexes in THF similarly to the Li complexes. Also, in all the dynamic ^{13}C NMR spectra, only one set of signals for the Cp-ring carbons was observed,

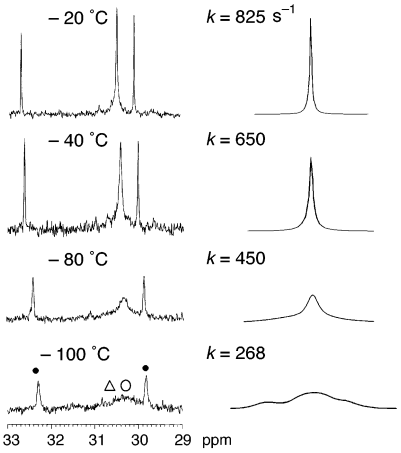

Figure 10. Temperature-dependent (a) experimental and (b) simulated ^{13}C NMR spectra of **2**−Na in THF-d_8. The signals marked with ○ and Δ correspond to methylene cabons, and that marked with ● corresponds to bridgehead carbons of the BCO units. [**2**−Na] = 0.055 M.

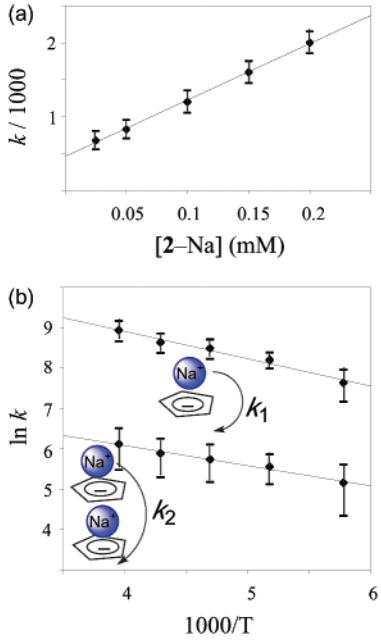

Figure 11. (a) Dependence of the observed rate k upon [**2**−Na] (T = 258 K) and (b) Arrhenius plot of the kinetic data obtained by the line-shape analysis (Figure 10) and eq 7 in THF-d_8; k_1 in s^{-1}; k_2 in L mol^{-1} s^{-1}.

indicating that the equilibrium with the SSIP or sandwich-type dimer was also negligible in Na and K complexes.

Among these complexes, phenyl-substituted derivatives **1**−Na and **1**−K showed no detectable dependence on the concentration of **1**−M ranging from 0.05 to 0.2 M, suggesting that the internal exchange is dominant, just as in the case of **1**−Li. In contrast, the exchange rate of **2**−Na and **2**−K was found to increase in a linear relationship with the concentration of **2**−M, as shown in Figures 11a and 13a. From these results, the observed $k_{(\mathbf{2}-\mathrm{M})}$ can be expressed as eq 7:

$$k_{(\mathbf{2}-\mathrm{M})} = k_{1(\mathbf{2}-\mathrm{M})} + k_{2\,(\mathbf{2}-\mathrm{M})}[\mathbf{2}-\mathrm{M}] \qquad (\mathrm{M} = \mathrm{Na}, \mathrm{K}) \quad (7)$$

The rate constant k_1 obtained from eq 7, i.e., the intercept in the linear plots of k against the concentration of **2**−M, should correspond to the rate for the concentration-independent intramolecular process, i.e., the internal site exchange. On the other

hand, the rate constant k_2, obtained as the inclination of the plot, should reflect the intermolecular process, i.e., the external site exchange such as that proceeding through formation of a sandwich-type dimer in the transition state. The kinetic data (k_1 and k_2) for **1**−Na and **2**−Na and for **1**−K and **2**−K are shown in Tables 6 and 7. The Arrhenius plots of the kinetic data for both $k_{1(2-M)}$ and $k_{2\ (2-M)}$ are shown in Figures 11b and 13b.

The thermodynamic parameters thus obtained for Na and K complexes of **1** and **2** are also shown in Table 3. The values of $\Delta H^{\ddagger}$ and $\Delta S^{\ddagger}$ include relatively large errors for **1**−K and **2**−Na. Therefore, the discussion of the dynamic behavior of Li, Na, and K complexes of **1** and **2** will hereafter be made on the basis of the values of $\Delta G^{\ddagger}$. Upon comparison of the results obtained from the rate constant k_1 (internal exchange), it is to be noted that the values for $\Delta G^{\ddagger}$ are quite similar for **1**−Li (12.6 ± 0.1 kcal mol^{-1}), **1**−Na (12.1 ± 0.2 kcal mol^{-1}), and **1**−K (12.0 ± 0.4 kcal mol^{-1}).

The kinetic process for k_1 is considered to consist of the following steps: that is, (1) a change from CIP to SSIP, which involves the dissociation of Cp−M to Cp$^-$ and M$^+$ with the simultaneous solvation of both ions; (2) site exchange of the M$^+$ ion within the SSIP in the transition state; and (3) recombination to give the Cp−M complex with the M$^+$ ion at the site opposite to the original complex. The observed value of $\Delta G^{\ddagger}$ is apparently related to steps 1 and 2, and step 1 can be simply divided into the dissociation of Cp−M and the solvation of the resulting ions. Theoretical calculations (B3LYP/6-31G(d)) then afford the following values for the dissociation step (eqs 8 and 9):

$$\mathbf{1}\text{−M} \rightarrow \mathbf{1} + \text{M}^+ \qquad (8)$$

ΔE_8 (M = Li, 162.7 kcal mol^{-1}; Na, 131.6 kcal mol^{-1}; K, 110.9 kcal mol^{-1})

$$\mathbf{2}\text{−M} \rightarrow \mathbf{2} + \text{M}^+ \qquad (9)$$

ΔE_9 (M = Li, 170.0 kcal mol^{-1}; Na, 137.5 kcal mol^{-1}; K, 115.4 kcal mol^{-1})

Apparently the dissociation energy decreases by 20 to 30 kcal mol^{-1} as the size of the alkali metal becomes larger. On the other hand, the calculations predict the following stabilization energies for solvation of the metal ion:

$$\text{M}^+ + 4(\text{Me}_2\text{O})_4 \rightarrow \text{M}^+(\text{Me}_2\text{O})_4 \qquad (10)$$

ΔE_{10} (M = Li, −122.9 kcal mol^{-1}; Na, −94.7 kcal mol^{-1}; K, −67.7 kcal mol^{-1})

These calculated energies of the solvation are in reasonable qualitative agreement with the experimentally determined values (Li, −104.7 kcal mol^{-1};[23a] Na, −71.1 kcal mol^{-1};[23b] K, −56.9 kcal mol^{-1} [23c]) and are again shown to decrease as the size of the metal increases. Therefore, the higher dissociation energy in Cp−M for the smaller metal ion is counterbalanced by the higher stabilization of the solvation of the metal ion.[20] This compensation results in the small difference in the calculated energy for dissociation of solvent-coordinated **1**−M or **2**−M into Cp$^-$ and solvent-coordinated M$^+$ in eq 11 (summarized in Table 8), which is in agreement with the experimentally observed small difference in the $\Delta G^{\ddagger}$ value of the internal exchange for all the Cp−M complexes. Consequently, this also implies that the difference in $\Delta G^{\ddagger}$ for the metal-ion site exchange (step (2)) in SSIP would be negligible

$$\text{Cp−M}(\text{Me}_2\text{O})_3 + \text{Me}_2\text{O} \rightarrow \text{Cp}^- + \text{M}^+(\text{Me}_2\text{O})_4 \qquad \Delta E_{11}$$

$$(\text{Cp}^- = \mathbf{1}, \mathbf{2}) \qquad (11)$$

As for the intermolecular process (k_2), the transition state would possibly involve the sandwich-type dimer. To see the feasibility of such dimer formation, the optimized structure of

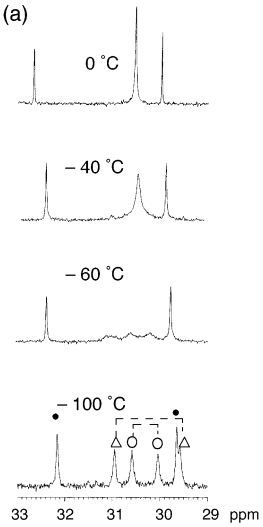

Figure 12. Temperature-dependent (a) experimental and (b) simulated ^{13}C NMR spectra of **2**−K in THF-d_8. The signals marked with O and Δ correspond to methylene cabons and that marked with • corresponds to bridgehead carbons of the BCO units. [**2**−K] = 0.05 M.

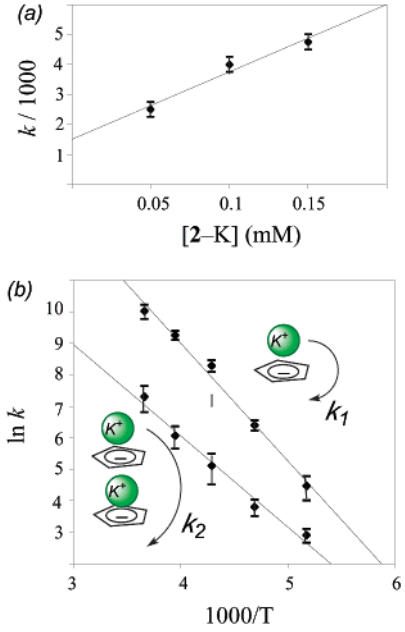

Figure 13. (a) Dependence of the observed rate k upon [**2**−K] (T = 278 K) and (b) Arrhenius plot of the kinetic data obtained by the line-shape analysis (Figure 12) and eq 10 in THF-d_8; k_1 in s^{-1}; k_2 in L mol^{-1} s^{-1}.

(23) (a) More, M. B.; Glendening, E. D.; Ray, D.; Feller, D.; Armentrout, P. B. *J. Phys. Chem.* **1996**, *100*, 1605−1614. (b) More, M. B.; Ray, D.; Armentrout, P. B. *J. Phys. Chem. A* **1997**, *101*, 831−839. (c) More, M. B.; Ray, D.; Armentrout, P. B. *J. Phys. Chem. A* **1997**, *101*, 4254−4262.

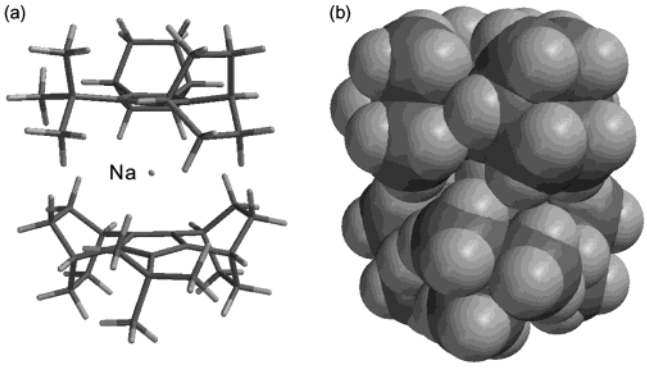

Figure 14. Optimized structure (B3LYP/6-31G(d)) of (**2**−Na−**2**)$^-$ expressed as (a) a stick model and (b) a space filling model.

the sandwich dimer (**2**−M−**2**)$^-$ was calculated at the B3LYP/6-31G(d) level of theory, together with (**1**−M−**1**)$^-$ for comparison. Of these, the optimized structure of (**2**−Na−**2**)$^-$ is shown in Figure 14 as an example (for the optimized structures of the rest of (**1**−M−**1**)$^-$ and (**2**−M−**2**)$^-$ see the Supporting Information). In the structure shown in Figure 14, the two *tert*-butyl groups take a staggered orientation to minimize the steric hindrance. The Na^+ ion is sandwiched by the two Cp^- rings with the averaged distance for C_{Cp}−Na of 2.75 Å. This distance is comparable to the observed value (2.63 Å) previously reported for the (Cp−Na−Cp)$^-$ complex.[24] The energy for formation of the sandwich-type dimer from the solvent-coordinated complex Cp−M(Me$_2$O)$_3$, including both **1** and **2**, defined as eq 12, was calculated, and the results are also shown in Table 8

$$2\ \mathrm{Cp{-}M(Me_2O)_3} \rightarrow (\mathrm{Cp{-}M{-}Cp})^- + 2\ \mathrm{Me_2O} + \mathrm{M^+(Me_2O)_4} \qquad \Delta E_{12} \quad (12)$$

The dimer formation in eq 12 was calculated to be highly endothermic. This would also be principally due to neglect of the stabilizing interaction between the dimer anion and the solvent-coordinated cation, $M^+(Me_2O)_4$. With regard to this, the stabilization caused by an interaction between the lithocene-type dimer of isodicyclopentadienide and $Li^+(H_2O)_4$ in SSIP was shown to be −46.2 kcal mol^{-1}, according to the results of previously reported MNDO calculations.[4] The values of ΔE_{12} calculated for all the complexes Cp−M were found to be almost identical, regardless of the kind of metal (M) and Cp (**1** and **2**). In contrast, for the process expressed in eq 11, the dissociation energy ΔE_{11} increased as the size of the metal increased, and the values for the *tert*-butyl derivative **2** are larger than those for the phenyl derivative **1**. Therefore, assuming that the stabilization energy due to the interaction between M^+ and Cp^- or M^+ and (Cp−M−Cp)$^-$ in SSIP is similar irrespective of the type of the metal,[25] the calculation results appear to indicate that the dimer formation becomes more facile as the size of the metal increases and is more favorable in **2** than in **1**. These calculation results are consistent with the acceleration of site exchange by an intermolecular process being observed only for **2**−Na and **2**−K, and therefore the transition state of the intermolecular process was likely to involve the sandwich-type dimer. Finally, we note that the formation of lithocene has been shown to be unfavorable compared with sodocene by the previous ab initio calculations.[24] This finding can be explained by the stronger repulsive interaction between the Cp rings in the lithocene anion, which is due to the smaller Cp−Li distance. This calculation result is also consistent with our present observation that the intermolecular exchange was not detected in the dynamic process of **2**−Li.

(24) Harder, S.; Prosenc, M. H.; Rief, U. *Organometallics* **1996**, *15*, 118−122.
(25) Such an assumption seems reasonable because, in the SSIPs, there would not be much difference in the distance between the positively charged metal and the negatively charged Cp ring, which are separated only by the common solvent of the same size and would be almost identical irrespective of the type of the metal.

Conclusion

We have for the first time succeeded in the direct NMR observation of dynamic behaviors of Cp−Na and Cp−K complexes in THF-d_8 solution by the use of the structural modification of the Cp ring with bicyclic frameworks. The Cp−alkali metal complexes **1**−M and **2**−M were found to form monomeric CIPs in the ground state, and the metals of CIPs are considered to exchange position between the upper and lower faces of the Cp ring dominantly via an intramolecular process in solution. The difference in the activation energy for this intramolecular exchange process was found to be quite small (less than 2 kcal mol^{-1}) for the complexes **1**−M and **2**−M (M = Li, Na, K), with a slight tendency to increase with decreases in the size of the metal. This is in contrast to the large difference in dissociation energy calculated for these complexes with increases in the metal size (by 20−30 kcal mol^{-1} for the change of Li → Na and Na → K). This large difference seems to be counterbalanced by the change in the solvation energy of each of the dissociated metal ions, which should be larger for smaller metal ions, as has also been demonstrated by theoretical calculations.

Experimental Section

General. ^{1}H and ^{13}C NMR spectra were recorded on a Varian Mercury-300 spectrometer. Variable temperature ^{13}C and ^{7}Li NMR measurements were performed on a JEOL JNM-AL400 spectrometer. Chemical Shifts of ^{1}H and ^{13}C NMR are reported in parts per million with reference to tetramethylsilane using the signals of $CHCl_3$ or α-CH_2 of THF as an internal standard (δ 7.26 or 3.58 in ^{1}H NMR and δ 77.0 or 67.4 in ^{13}C NMR, respectively), while the external standard of LiBr was used in ^{7}Li NMR. Mass spectra (EI) were taken on JEOL JMS-HX110 or JMS700 spectrometers.

All reactions were conducted under a dry argon atmosphere unless otherwise indicated. Ether, THF, and, toluene were distilled over benzophenone ketyl under N_2 atmosphere. Lithium diethylamide was prepared from diethylamine and *n*-BuLi in hexane and dried under high vacuum. Commercially available sodium amide (50 wt % suspension in toluene) and potassium hydride (30% in mineral oil) were washed several times with dry pentane in a dry glovebox before use. Alumina (ICN alkali activated grade I) was deactivated by adding 6 wt % of water and vigorously shaking. Other reagents were used as received without further purification.

Method of Calculations. Optimization of structures was performed using Gaussian 98 programs[26] at B3LYP/6-31G(d) levels of density

(26) Frisch, M. J.; Trucks, G. W.; Schlegel, H. B.; Scuseria, G. E.; Robb, M. A.; Cheeseman, J. R.; Zakrzewski, V. G.; Montgomery, Jr., J. A.; Stratmann, R. E.; Burant, J. C.; Dapprich, S.; Millam, J. M.; Daniels, A. D.; Kudin, K. N.; Strain, M. C.; Farkas, O.; Tomasi, J.; Barone, V.; Cossi, M.; Cammi, R.; Mennucci, B.; Pomelli, C.; Adamo, C.; Clifford, S.; Ochterski, J.; Petersson, G. A.; Ayala, P. Y.; Cui, Q.; Morokuma, K.; Malick, D. K.; Rabuck, A. D.; Raghavachari, K.; Foresman, J. B.; Cioslowski, J.; Ortiz, J. V.; Stefanov, B. B.; Liu, G.; Liashenko, A.; Piskorz, P.; Komaromi, I.; Gomperts, R.; Martin, R. L.; Fox, D. J.; Keith, T.; Al-Laham, M. A.; Peng, C. Y.; Nanayakkara, A.; Gonzalez, C.; Challacombe, M.; Gill, P. M. W.; Johnson, B.; Chen, W.; Wong, M. W.; Andres, J. L.; Gonzalez, C.; Head-Gordon, M.; Replogle, E. S.; Pople, J. A. *Gaussian 98*, Revision A.5; Gaussian, Inc.: Pittsburgh, PA, 1998.

functional theory. For determination of the energy difference in eqs 1−4 and 8−12, the total energies for each optimized structure were used.

Phenylcyclopentadiene 5. A 1.6 M solution of *tert*−BuLi in pentane (20 mL, 32 mmol) was added dropwise to a stirred solution of 2-bromobicyclo[2.2.2]octene[10b] (2.99 g, 16.0 mmol) in 30 mL of dry ether under argon at 0 °C. After stirring for 5 min at 0 °C, benzoyl chloride (0.95 mL, 8.18 mmol) was added dropwise. The mixture was stirred for 10 min and then allowed to warm to room temperature. After stirring for 2 h, the reaction was quenched with water and the mixture was extracted with ether and dried over $MgSO_4$. Removal of the solvent in vacuo gave crude 3-phenyl-1,4-pentadien-3-ol derivative **3** (2.5 g, 98%) as a pale yellow oil: ^{1}H NMR (300 MHz, $CDCl_3$) δ 7.5−7.2 (m, 5H), 6.00 (dd, 2H), 2.61 (bs, 2H), 2.52 (bs, 2H) 1.6−0.8 (m, 16H). The crude **3** was sensitive to an acid and used for next step without further purification. To a solution of **3** (2.5 g, 7.8 mmol) in 40 mL of ether under argon at room temperature was added dropwise a solution of *p*-toluenesulfonic acid (166.4 mg, 0.876 mmol) in 40 mL of ether quickly, and the mixture was stirred for 1 h. After removal of the solvent in vacuo, the mixture was purified by column chromatography over deactivated Al_2O_3 eluted with hexane to give **5** (1.36 g, 56.2%) as a colorless solid: mp 98−100 °C; ^{1}H NMR (300 MHz, $CDCl_3$) δ 7.30 (m, 2H), 7.28 (m, 2H), 7.08 (m, 1H), 3.64 (s, 1H), 3.16 (t, 1H), 2.77 (t, 1H), 2.70 (t, 1H), 2.18 (bs, 1H), 2.0−0.7 (m, 16H); ^{13}C NMR (75.5 MHz, $CDCl_3$) δ 149.2, 144.9, 143.0, 137.6, 132.4, 128.4, 126.6, 124.6, 59.1, 34.3, 31.8, 29.2, 29.0, 28.0, 27,0, 26.6, 26.1 (two signals were overlapped), 25.9, 24.6, 22.1. HRMS (EI) calcd for $C_{23}H_{26}$ 302.2035, found 302.2024. Anal. Calcd for $C_{23}H_{26}$: C, 91.34; H8.66. Found: C, 91.05; H, 8.75.

***tert*-Butylcyclopentadiene 6.** A 1.6 M solution of *tert*−BuLi in pentane (6.5 mL, 10.4 mmol) was added dropwise to a stirred solution of 2-bromobicyclo[2.2.2]octene[10b] (0.97 g, 5.2 mmol) in 10 mL of dry ether under argon at 0 °C. After stirring for 5 min at 0 °C, pivaloyl chloride (0.32 mL, 2.6 mmol) was added dropwise. The mixture was stirred for 10 min and then allowed to warm to room temperature. After stirring for 2 h, the reaction was quenched with water, and then the reaction mixture was extracted with ether and the ethereal solution dried over $MgSO_4$. Removal of the solvent in vacuo gave crude **4** (0.78 g, 98%) as a pale yellow oil: ^{1}H NMR (300 MHz, $CDCl_3$) δ, 6.16 (dd, 2H), 2.75 (bs, 2H), 2.51 (bs, 2H) 1.6−0.8 (m, 8H), 1.03 (s, 9H). The crude **4** was sensitive to an acid and used for next step without further purification. A solution of **4** (0.78 g, 2.6 mmol) in 50 mL of toluene was refluxed over $KHSO_4$ (173.7 mg, 1.27 mmol) for 24 h. After removal of the solvent in vacuo, the mixture was purified by column chromatography over deactivated Al_2O_3 eluted with hexane to give **6** (246 mg, 34%) as a colorless solid: mp 92−94 °C; ^{1}H NMR (300 MHz, $CDCl_3$) δ 3.14 (s, 1H), 3.00 (m, 1H), 2.66 (m, 1H), 2.57 (m, 1H), 2.42 (bs, 1H), 2.0−0.7 (m, 16H) 1.22 (s, 9H); ^{13}C NMR (75.5 MHz, $CDCl_3$) δ 145.0, 142.7, 140.9, 139.5, 59.8, 33.9, 33.5, 32.9, 31.6, 30.0, 28,6, 27.9, 27.2, 26.9, 25.99, 25.96, 25.85, 24.8, 21.6. HRMS (EI) calcd for $C_{21}H_{30}$ 282.2348, found 282.2350. Anal. Calcd for $C_{21}H_{30}$: C, 89.30; H10.70. Found: C, 89.51; H, 10.79.

Preparation of 1-M and 2-M. A General Procedure. In a dry glovebox, appropriate amount (10−45 mg; 0.038−0.15 mmol) of **5** or **6** and 1.0 equiv of a base ($LiNEt_2$, $NaNH_2$, or KH) were placed into an NMR tube connectable to a vacuum line. The tube was evacuated, and then 0.75 mL of THF-d_8, which had been dried over Na−K alloy and had degassed by three freeze−pump−thaw cycles, was vapor-transferred directly into the tube cooled with liquid nitrogen. After all of the solvent was transferred, the tube was sealed under vacuum. The solution of the mixture of **6** and $LiNEt_2$ was warmed at 50 °C for 2 h to give **2**−Li. The suspension of the mixture of **5** or **6** and $NaNH_2$ was sonicated for 1 or 50 h to give **1**−Na or **2**−Na, respectively. The reactions of the other mixtures (**5** and $LiNEt_2$) (**5** or **6** and KH) were found to be completed within 5 min at room temperature.

1−Li: ^{1}H NMR (300 MHz, THF-d_8) δ 7.28 (m, 2H), 7.11 (m, 2H), 6.75 (m, 1H), 3.34 (bs, 2H), 2.96 (bs, 2H), 1.74 (m, 8H), 1.30 (m, 8H); ^{13}C NMR (75.5 MHz) δ 142.7, 128.1, 127.5, 120.8, 118.0, 117.7, 108.3, 30.5, 30.5(br), 30.0(br), 29.8. ^{7}Li NMR (153.7 MHz) δ −7.34.
1−Na: ^{1}H NMR (300 MHz, THF-d_8) δ 7.27 (m, 2H), 7.02 (m, 2H), 6.58 (m, 1H), 3.33 (bs, 2H), 2.96 (bs, 2H), 1.71 (m, 8H), 1.30 (m, 8H); ^{13}C NMR (75.5 MHz) δ 144.4, 128.1, 126.5, 119.0, 118.9, 118.5, 107.1, 31.3, 30.4(br), 30.3(br), 30.2.
1−K: ^{1}H NMR (300 MHz, THF-d_8) δ 7.20 (m, 2H), 7.02 (m, 2H), 6.57 (m, 1H), 3.33 (bs, 2H), 2.96 (bs, 2H), 1.73 (m, 16H), 1.27 (s, 8H); ^{13}C NMR (75.5 MHz) δ 144.7, 128.2, 126.4, 118.6, 108.3, 31.0, 30.3, 30.2, 30.1.
2−Li: ^{1}H NMR (300 MHz, THF-d_8) δ 3.28 (bs, 2H), 2.88 (bs, 2H), 1.9−0.8 (m, 16H), 1.35 (s, 9H); ^{13}C NMR (75.5 MHz) δ 115.9, 115.2, 114.5, 34.9, 34.8, 31.9, 31.5, 30.8, 30.2, 29.8, 29.1. ^{7}Li NMR (153.7 MHz) δ -8.60.
2−Na: ^{1}H NMR (300 MHz, THF-d_8) δ 3.27 (bs, 2H), 2.86 (bs, 2H), 1.9−0.8 (m, 16H), 1.35 (s, 9H); ^{13}C NMR (75.5 MHz) δ 116.0, 114.5, 113.0, 35.3, 32.9, 30.6, 30.1.
2−K^{1}H NMR (300 MHz, THF-d_8) δ 3.28 (bs, 2H), 2.88 (bs, 2H), 1.9−0.8 (m, 16H), 1.35 (s, 9H); ^{13}C NMR (75.5 MHz) δ 115.7, 114.3, 113.0, 35.4, 35.1, 32.8, 30.6, 30.0.

X-Ray Structural Determination. In exactly the same way as that for the preparation of NMR samples, ca. 0.2 M solutions of **1**−Li, **1**−Na, and **2**−Na in 1.0 mL of dry THF were prepared in glass tubes (inner diameter 5 mm × 15 cm) and sealed under vacuum. Colorless crystals of the corresponding Cp−M(THF)$_3$ complexes were found to be grown near the surfaces of these solutions, which were let stand at −20 °C for 4−6 days. After breaking the tubes, the crystals were transferred into silicone oil, and single crystals suitable for X-ray analysis were selected as quickly as possible by the use of a Hampton Research Cryo Loop under a microscope. The single crystal was quickly mounted on the magnetic base of a goniometer head in a nitrogen gas flow at −150 °C. For obtaining the single crystal of cyclopentadiene **5**, acetonitrile was slowly diffused into a nearly saturated solution of **5** in dichloromethane and the mixture was let stand at room temperature for 2 days. The intensity data were collected on a Bruker SMART APEX equipped with a CCD area detector with graphite monochromated MoKα radiation and graphite monochromator. Frames corresponding to an arbitrary hemispher of data were collected at −150 °C using ω scans of 0.3° counted for a total of 10 s per frame. The structure was solved by direct methods (SHELXTL) and refined by the full-matrix leastert-squares on F^2 (SHELEXL-97). All non-hydrogen atoms were refined anisotropically and all hydrogen atoms were placed using AFIX instructions.
1−Li(THF)$_3$: $C_{35}H_{49}LiO_3$; FW = 524.68, orthorhombic, P_{bca}, colorless, a = 10.4024(12) Å, b = 17.796(2) Å, c = 31.256(4) Å, Z = 8, R_1 = 0.0754, wR_2 = 0.2012 ($I > 2\sigma(I)$), GOF = 1.053.
1−Na(THF)$_3$: $C_{35}H_{49}NaO_3$; FW = 540.73, triclinic, P-1, colorless, a = 9.6261(9) Å, b = 10.5597(10) Å, c = 16.1138(15) Å, α = 76.720(2)°, β = 88.816(2)°, γ = 69.497(2)°, Z = 2, R_1 = 0.0513, wR_2 = 0.1294 ($I > 2\sigma(I)$), GOF = 1.048.
2−Na(THF)$_3$: $C_{33}H_{53}NaO_3$; FW = 520.74, triclinic, P-1, colorless, a = 9.6126(11) Å, b = 10.2370(12) Å, c = 16.5405(19) Å, α = 98.989(2)°, β = 102.266(2)°, γ = 107.440(2)°, Z = 2, R_1 = 0.0450, wR_2 = 0.1132 ($I > 2\sigma(I)$), GOF = 1.026.
5: $C_{23}H_{26}$; FW = 302.44, triclinic, P-1, colorless, a = 6.214(3) Å, b = 11.624(5) Å, c = 13.218(8) Å, α = 113.393(10)°, β = 100.585(11)°, γ = 98.552(7)°, Z = 2, R_1 = 0.0555, wR_2 = 0.1400 ($I > 2\sigma(I)$), GOF = 0.979.

Kinetic Measurements. To observe the chemical shifts for the split signals of methylene carbons, which were necessary in the line shape analysis, low-temperature ^{13}C NMR measurements were conducted in THF-d_8, at −60 °C for **1**−Li (0.05 M), at −10 °C for **2**−Li (0.2 M), and at −100 °C for **2**−K (0.05 M). However, sufficient splitting was not observed for **1**−Na, **1**−K, and **2**−Na in THF-d_8 even at −100 °C.

Thus, a 1:1 mixture of THF-d_8 and toluene-d_8 was used as s solvent to decelerate the metal-ion exchange process, and the split signals could be observed at −90 °C in the concentration of 0.01 M for **1**−Na, 0.01 M for **1**−K, and 0.25 M for **2**−Na. The observed ^{13}C NMR chemical shifts for the split methylene signals were as follows:
1−Li; 31.545, 31.083, 29.322, 28.562 ppm
1−Na; 30.959, 30.545, 30.008, 29.769 ppm
1−K; 30.669, 30.405, 29.909, 29.636 ppm
2−Li; 31.149, 30.504, 30.140, 29.719 ppm
2−Na; 31.322, 30.901, 30.140, 29.967 ppm
2−K; 31.008, 30.611, 30.091, 29.703 ppm

Acknowledgment. This work was supported by the Grant-in-Aid for COE Research on Elements Science (No. 12CE2005) from the Ministry of Education, Culture, Sports, Science and Technology, Japan. Computation time was provided by the Supercomputer Laboratory, Institute for Chemical Research, Kyoto University. H. S. thanks Alexander von Humboldt Foundation and the Japan Society for the Promotion of Science for the Postdoctoral Fellowship for Foreign Researchers.

Supporting Information Available: ^{1}H and ^{13}C NMR spectra of **1**−M and **2**−M (M = Li, Na, K), ^{7}Li NMR spectra of **1**−Li and **2**−Li, X-ray crystallographic data for crystals **1**−Li(THF)$_3$, **1**−Na(THF)$_3$, **2**−Na(THF)$_3$, and **5**, the results of line shape analysis and Arrehnius plot, and Cartesian coordinates and total energies for the optimized structures of all calculated molecules. This materials is available free of charge via the Internet at http://pubs.acs.org.

JA0346431